Major modes of climate variability dominate nonlinear Antarctic ice-sheet elevation changes 2002-2020

Matt A. King[1,2], Poul Christoffersen[2,3]

[1]Surveying and Spatial Sciences, School of Geography, Planning, and Spatial Sciences, University of Tasmania, Hobart, Tasmania 7001, Australia

[2]The Australian Centre for Excellence in Antarctic Science, University of Tasmania, Hobart, Tasmania 7001, Australia

[3]Institute for Marine and Antarctic Studies, University of Tasmania, Hobart, Tasmania 7001, Australia

Corresponding author: Matt King (Matt.King@utas.edu.au)

Key Points:

- Cumulative effects of large-scale climate modes dominate detrended altimeter time series of Antarctic ice elevation 2002-2020
- These decadal signals have the same spatial pattern in altimeter ice height and GRACE mass time series.
- These decadal signals are largely due to surface mass balance, but ice dynamic changes may play a role in the Amundsen Sea Embayment

Abstract

We explore the links between elevation variability of the Antarctic Ice Sheet (AIS) and large-scale climate modes. Using multiple linear regression, we quantify the time-cumulative effects of El Niño Southern Oscillation (ENSO) and the Southern Annular Mode (SAM) on gridded AIS elevations. Cumulative ENSO and SAM explain a median of 29% of the partial variance and up to 85% in some coastal areas. After spatial smoothing, these signals have high spatial correlation with those from GRACE gravimetry (r~=0.65 each). Much of the signal is removed by a firn densification model but inter-model differences exist especially for ENSO. At the lower parts of the Thwaites and Pine Island glaciers, near their grounding line, we find the Amundsen Sea Low (ASL) explains ~90% of the observed elevation variability. There, modeled firn effects explain only a small fraction of the variability, suggesting significant height changes could be a response to climatological ice-dynamics.

Plain Language Summary

This study investigates how variations in the height of the Antarctic Ice Sheet (AIS) are connected to large-scale climate patterns. We used a statistical method to measure the effects of two climate phenomena: El Niño Southern Oscillation (ENSO) and the Southern Annular Mode (SAM). We found that the cumulative effects of these phenomena account for about 29% of the variations in AIS height on average, and up to 85% in some coastal areas. These patterns match well with independent data from the GRACE satellites over the same period. Applying a model that considers the accumulation of snow and its compaction into ice (firn densification) removes much of this signal, suggesting much, but not all, of the signals are related to snowfall variations. At the fronts of the rapidly changing Thwaites and Pine Island glaciers, the dominant climate phenomenon is the Amundsen Sea Low (ASL), which varies in strength and location. Here, the cumulative effects of the ASL changes explain about 90% of the variations in height of these glaciers, with only a small part explained by firn effects. We suggest the unexplained variability could be partly due to changes in ice flow.

1 Introduction

Observations of the changing volume of the Antarctic Ice Sheet play a major role in understanding ice-sheet change (e.g., Otosaka et al., 2023; Shepherd et al., 2012) from the whole-of-ice-sheet down to individual glaciers (e.g., Smith et al., 2020; Wingham et al., 2009). The now three-decade record of continuous ice volume change captures the variability and longer-term change of both surface mass balance (SMB), and related firn processes, and elevation effects of changing ice dynamics. These changes are, respectively, related to atmospheric and oceanic processes (Horwath et al., 2012; Smith et al., 2020). Several studies have examined the relationship between ice height changes and modes of climate variability, in particular linking them to both El Niño - Southern Oscillation (ENSO) and the Antarctic Circumpolar Wave (Kaitheri et al., 2021; Mémin et al., 2015; Mémin et al., 2014).

Less studied in this context is the role of the dominant mode of climate variability in the Southern Hemisphere, the Southern Annular Mode (SAM). Despite SAM driving variability and trends in SMB across a wide range of timescales (Diener et al., 2021; Medley & Thomas, 2019;

van den Broeke & van Lipzig, 2017), SAM has yet to be linked to observations of ice sheet elevation change, with one related study reporting no correlation to estimates of ice shelf elevation change (Paolo et al., 2018). By contrast, the cumulative sum of SAM (Diener et al., 2021; Kim et al., 2020) has recently been shown to be linearly related to the dominant signal in detrended surface mass time series derived from satellite gravimetry (King et al., 2023), with large-scale spatially-coherent signal across coastal regions at decadal timescales.

The ~300 km spatial resolution of satellite gravimetry, combined with uncertainties in models of SMB (Mottram et al., 2021), meant that King et al. (2023) were not able to separate the relative contributions of SMB and ice dynamical change forced respectively by the atmosphere and ocean (Hansen et al., 2021; Kim et al., 2020; Palóczy et al., 2018; Spence et al., 2017; Thomas et al., 2017; Verfaillie et al., 2022). In particular, ice dynamical change will have a distinct spatial pattern compared to SMB that is not detectable by GRACE but could be possible with altimetry (Smith et al., 2020). Detecting (or otherwise) a response of the grounded ice sheet to large-scale climate variability via the oceans and ice shelves would provide important insights into ice-sheet sensitivity to climate change.

In this paper we analyze a recent gridded compilation of satellite altimeter data and compare these time series to cumulative climate indices. We compare the derived signals to those from space gravimetry and then, taking advantage of the high-resolution altimeter data, explore the signal over key ice streams: Thwaites, Pine Island, Totten, and Denman.

2 Datasets and Analysis

2.1 Altimeter dataset

We make use of a gridded altimeter product (Nilsson et al., 2023) at 1920 m horizontal resolution and covering the period from Apr 1985 to Dec 2020 (Nilsson et al., 2022). We spatially down-sample this to 5 km horizontal resolution. To facilitate comparison with space gravimetry data we only make use of data from 2002 to the end of the record. The dataset contains monthly ice-sheet elevation-change data derived from a range of radar and laser altimeter missions; over the study period these are ERS-2, Envisat and CryoSat-2 and ICESat and ICESat-2. The approach to accounting for differences in reflection surfaces and other systematic effects is described by Nilsson et al. (2022). To reduce spatial noise, we apply a Gaussian smoother with widths specified in later sections. For these, width is defined at the half height of the Gaussian function, consistent with the definition commonly used in GRACE data smoothing (Wahr et al., 1998).

2.2 Space gravimetry dataset

We use the COST-G RL01 Level-3 50 km gridded ice-mass change per surface area GRACE and GRACE-FO V0002 dataset obtained from http://gravis.gfz-potsdam.de/antarctica (Sasgen et al., 2020). We make use of data from Mar 2002 to Dec 2020, with the end point chosen to match

the end of the altimetry dataset. The data are spaced approximately monthly and with a data gap of ~12 months between GRACE and GRACE-FO from mid-2017 to mid-2018.

We note that while this product is gridded at 50 km, the intrinsic GRACE resolution is ~300-400 km. Post-processing steps include replacement of low-degree GRACE coefficients and insertion of degree-1 terms using standard approaches (Dahle & Murböck, 2020; Sasgen et al., 2020).

Since we are interested in decadal variability and trends, we also lightly smooth the altimetry and GRACE data with a Gaussian filter with width 7 months (Wahr et al., 1998).

2.3 Climate indices

We compare the altimeter and GRACE data primarily with SAM and ENSO indices, with additional comparison to Amundsen Sea Low (ASL) indices in the Amundsen Sea region. For the ASL indices, we make use of both the absolute center pressure (ASLP) and longitude (ASLλ) within the ASL Index version 3.20210820-era5 based on monthly ERA5 reanalysis data (Hosking et al., 2016). For SAM, we make use of the Marshall station index (Marshall, 2003). For ENSO, we make use of the Nino3.4 index based on the HadISST1 dataset (Rayner, 2003) and use a 6-month lag (King et al., 2023; Paolo et al., 2018). We normalized each index with the mean and standard deviation computed over 1971-1999 inclusive, then cumulatively summed them, limited them to the data period, and then renormalized to produce SAM_Σ, $ENSO_\Sigma$, $ASLP_\Sigma$, and $ASL\lambda_\Sigma$.

The raw indices and their cumulative sums are shown in Fig S1. Correlations above 0.7 are evident between $ASLP_\Sigma$ and SAM_Σ and between $ASL\lambda_\Sigma$ and $ENSO_\Sigma$ (Fig S1, S2). This is due to the ASL being affected by larger-scale modes of climate variability, with SAM in particular modulating its absolute pressure and ENSO modulating the longitude of its center (Clem et al., 2017; Hosking et al., 2016; Turner et al., 2013).

2.4 Multi-variate Empirical Orthogonal Functions

For a data-driven analysis we make use of Multi-variate Empirical Orthogonal Functions (MEOF) (Wang, 1992; Wu, 2023). MEOFs are an extension of conventional Empirical Orthogonal Functions but allow the dominant modes across multiple variables to be identified rather than treating each variable separately. We use MEOF to analyze the elevation and mass change gridded datasets after individual normalization. We first smooth the altimetry dataset with a 50 km-wide Gaussian smoother and sub-sample the altimeter dataset to match the 50 km horizontal grid resolution of GRACE. Given the limited sampling of altimetry in the northern Antarctic Peninsula we truncate that region from both datasets prior to computing MEOFs.

2.5 Regression

Using ordinary least squares, we solved the coefficients (a, b, c, d, and e) of the functional model describing time-evolving elevation (h) with time (t):

$$h(t_i) = a + b(t_i - t_0) + \sum_{k=1}^{2}(c_k^s \sin(2\pi f_k t_i) + c_k^c \cos(2\pi f_k t_i)) + dSAM_\Sigma + eENSO_\Sigma \quad (1)$$

Where f_k = [1, 2] cycles per year. We adopted t_0 as the mid point of the altimeter series.

2.6 Data uncertainty

For regression parameter uncertainties, we recognize the existence of temporal correlations in the altimeter time series (Ferguson et al., 2004), in part due to SMB variation (King & Watson, 2020), and take these into account. Following King et al. (2023), we compared trend uncertainties from a linear regression using a Generalized Gauss Markov noise model to those generated using a white noise only (temporally uncorrelated) noise model using HECTOR v2.0 software (Bos et al., 2013). For regressions that included the SAM and ENSO terms, the white noise only model produced uncertainties a factor of 3 too small, taken as the median of the ratio of trend uncertainties, or factor 40 too small when not including the SAM and ENSO terms. We applied these scale factors to the uncertainties from the regression. For the GRACE uncertainties we used the scale factors of King et al. (2023).

3 Results

3.1 Ice-sheet scale analysis

Our data-driven MEOF analysis shows that ice elevation and mass time series are both dominated by decadal-scale variability (Fig. S3c, f). Together, the two leading modes explain 65% of the non-linear variance of the combined and smoothed time series. Their corresponding principal components (PCs) correlate with detrended SAM_Σ (r=0.73) and 6-month lagged $ENSO_\Sigma$ (r=0.89). The $ASLP_\Sigma$ and $ASL\lambda_\Sigma$ terms are not of direct relevance at the ice-sheet scale given the limited geographical footprint of influence of the ASL, but also have high correlations with the data.

GRACE and altimetry MEOFs have a high spatial correlation (Fig. S3a-b, d-e; r=0.87 for MEOF1 and r=0.75 for MEOF2) suggesting they are sensing the same signal and are both dominated by coastal changes. The potential in the high-resolution altimetry record is particularly evident in MEOF1 where the spatially-diffuse signal in GRACE (Fig. S3a) is shown to be concentrated over small regions that coincide with the major ice streams of the Amundsen Sea Embayment and the coastline of the Bellingshausen Sea and Marie Byrd Land (Fig. S3b). We note that while MEOF3 (Fig. S4) is partly affected by striping in the GRACE field, characteristic of GRACE systematic error, coherent signal is evident between GRACE and altimetry along the coastlines of the Bellingshausen Sea, Marie Byrd Land and Wilkes Land, suggesting the signal is robust in those regions, although the variance explained (5%) is much smaller than MEOFs 1 and 2. A similar signal to PC3, with periodicities of ~4-7 years, has also been identified in analysis of GRACE (King et al., 2023) or GRACE and altimetry data (Mémin et al., 2015). Beyond MEOF3, the modes explain little variance (<4%) and are dominated by noise, at least for GRACE (Fig. S4d).

To quantify the SAM and ENSO contribution to ice sheet elevation change we regress the altimetry time series against SAM_Σ and $ENSO_\Sigma$ and the other parameters in Eq. 1. Here we use the gridded data after applying a 10 km Gaussian spatial filter. The 5 km gridded altimeter regression analysis shown in Fig. 1a,b reveals large-scale spatially coherent signal relating to SAM and ENSO around the coasts of Antarctica. Together, these two terms often explain more than 40% of the partial variance ($R^2_{partial}$) of the timeseries around the coast and into the interior,

with the partial variance the square of the partial correlation within which effects of the other regression terms are controlled. The median partial-variance explained across the ice sheet is 29% (Fig. 1c). The SAM_{Σ} coefficient is strongest in the Amundsen Sea Embayment where it centers on the Pine Island, Thwaites, Smith, and Pope Glaciers (Fig. S5a). The negative elevation signal in this region is linked to periods where positive SAM dominates negative SAM (positive SAM_{Σ}). Other strong signal exists along the coastal zone of the Bellingshausen Sea, Marie Byrd Land, and parts of coastal East Antarctica. A more diffuse signal is evident in the interior of West Antarctica and parts of East Antarctica (Fig. S6a). The $ENSO_{\Sigma}$ coefficient has particularly high positive values, indicating elevation increase associated with sustained El Niño, along the coast of the Bellingshausen Sea and well upstream into Pine Island Glacier (Fig. S5b)

Applying a 200 km Gaussian smoother to the altimeter data and rerunning the regression (Fig. 1d-e) produces coefficients with large-scale spatial coherence and larger partial variances explained, often exceeding 60% in key coastal regions but extending well into the interior of the ice sheet (Fig. 1f). Comparing them to results of a regression with GRACE data (Fig. 1g-h) (King et al., 2023) shows high agreement in the signs and spatial distribution of the signal. We note that there are insufficient altimeter data in the Northern Antarctic Peninsula to analyze the signal in this region. Computing spatial correlations between the smoothed altimetry regression and the GRACE regression gives $r=0.65$ for SAM_{Σ} and $r=0.68$ for $ENSO_{\Sigma}$.

We next examine the role of SMB variability on the estimated coefficients from the altimetry regression. To do this we subtract the IMAU Firn Densification Model (IMAU FDM) v1.2A (Veldhuijsen et al., 2023) from the altimetry time series and repeat the regression. The results are shown in Figure 2. Comparing Fig. 2a with Fig. 1a shows that IMAU FDM effectively removes all the SAM-related signal in East Antarctic Ice Sheet (EAIS) but much of the SAM signal remains in West Antarctic Ice Sheet (WAIS). Much of the coastal EAIS ENSO-related signal is removed by IMAU FDM but with small over-correction evident for much of the ice sheet, including signal reversing sign in George V Land and WAIS. Repeating the regression but instead using the GSFC FDM v1.2.1 (Medley et al., 2022) shows that there is significant sensitivity to the choice of FDM (Fig. 2d-f), with GSFC FDM apparently over-correcting ENSO-related signal in the Totten Glacier region but in much better agreement with the altimetry in WAIS. Given the decadal timescales of the signals, these inter-model differences are likely to have contributions from both the FDMs themselves and their underlying SMB models (Medley et al., 2022; Verjans et al., 2021).

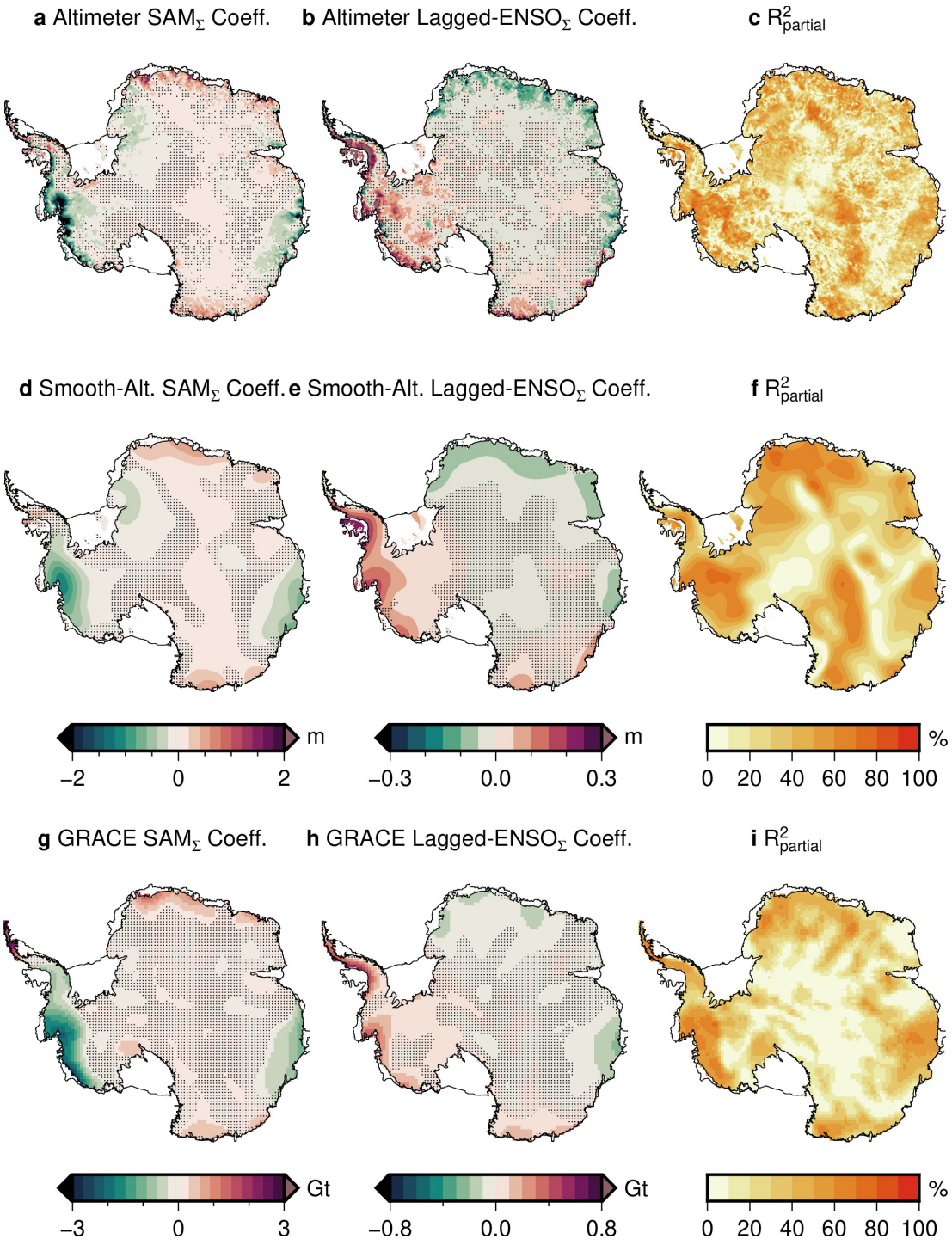

Figure 1. Results of regression analysis of gridded data. Shown are the SAMΣ and ENSOΣ coefficients and variances explained for the altimetry (top row), altimetry after 200 km Gaussian smoothing (middle row), and GRACE (bottom row). The partial variances explained by SAMΣ and lagged ENSOΣ are in the right column. The hachuring indicates regions not significantly different to zero at the 95% confidence interval.

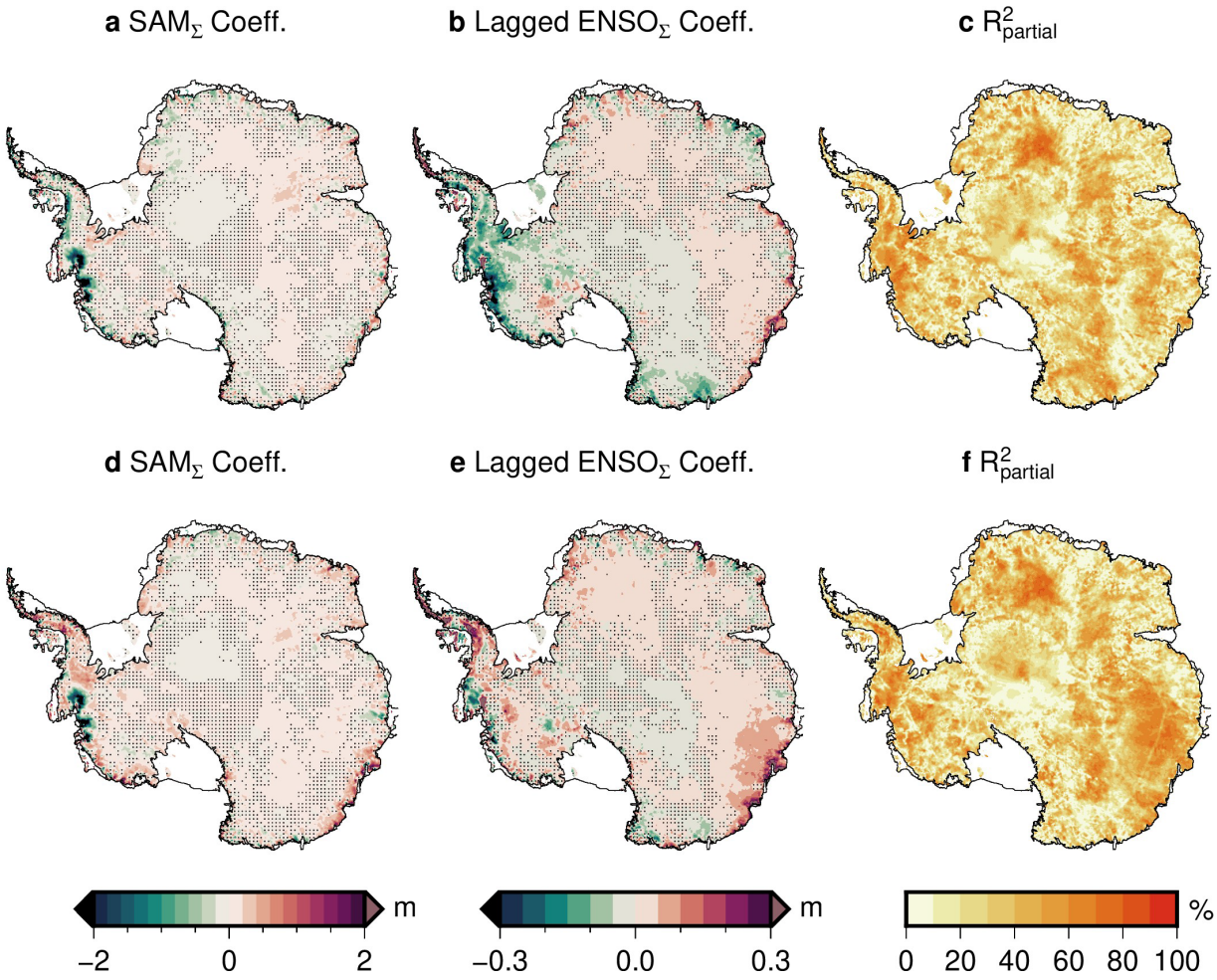

Figure 2. Results of regression analysis of FDM-corrected gridded altimeter data. Regression coefficients are shown (left and central columns) and the partial variances explained by SAMΣ and lagged ENSOΣ (right column). Shown are the coefficients and variances explained for the altimetry time series after subtracting of the IMAU FDM (top row) and GSFC FDM (bottom row).

Next, we explore the origins of these signals further on a glacier-by-glacier basis.

3.2 Regional scale analysis

3.2.1 Thwaites and Pine Island glaciers

The partial variance explained by the SAMΣ and ENSOΣ terms (before subtracting an FDM) is above 60% for much of the Amundsen Sea Embayment (ASE; Fig. 1c, f; S5c). Regardless of the FDM model adopted, much SAMΣ signal remains in the ASE broadly and ENSOΣ signal is evident in the Pine Island Glacier (PIG) region (Fig. 2). Closer examination of these regions in Fig. S5 (top row) indicates that the ASE signals are concentrated along low-elevation and fast

flowing regions that correspond to PIG, Thwaites, and nearby glaciers. This is further evidenced through cross-sections near to the front of these glaciers (Fig. S6) along the yellow lines in Fig S5. It is notable that the phase of the SAM-related signal is switched in the low elevation and fast-flowing region of PIG.

Coefficient magnitudes generally decay upstream of the grounding line (Fig. S7). Subtracting the IMAU FDM before performing the regression results in coefficients along the centerline and cross profiles that are shifted nearly uniformly but are not significantly altered in their spatial pattern (dashed lines Fig. S6-S7).

Along the coastal margin of the ASE the climatology is more directly controlled by the ASL than SAM and ENSO which modulate its depth and location (Clem et al., 2017; Turner et al., 2013). To explore this further we repeated the regression replacing SAM_{Σ} and $ENSO_{\Sigma}$ in Equation 1 with $ASLP_{\Sigma}$ and $ASL\lambda_{\Sigma}$. While the magnitude of the estimated coefficients differs between SAM_{Σ}/-$ASLP_{\Sigma}$ and $ENSO_{\Sigma}$/-$ASL\lambda_{\Sigma}$ the broader spatial pattern will be nearly identical due to the high correlations of these coefficient pairs over the data period (Fig. S1-S2) and so we just explore in detail the impact of estimating the ASL coefficients at one point location per glacier, at a centerline location about 20 km upstream of their respective grounding lines (Fig. S5 yellow crosses; Table S1).

The detrended data are shown in Fig. 3 (top row) where they reveal non-linear variability of several meters over the data period (blue plusses). Time series of estimated ASL coefficients sum to closely reproduce the data (black line). These two terms explain 84% (Thwaites) and 90% (Pine Island) of the partial variance of the altimeter time series. Interestingly, the phase of the $ASLP_{\Sigma}$ term is opposite between Thwaites and PIG, while the $ASL\lambda_{\Sigma}$ term is in phase.

Neither of the FDM models can explain the elevation variability at Thwaites or Pine Island glaciers (Fig. S8, brown lines). This could be because the SMB models are unable to reproduce the precipitation in this region, especially in ~2007 at Thwaites Glacier, but this would require a highly localized signal as this event does not occur at PIG. This is not implausible given existing SMB model limitations in low-altitude coastal regions (Kappelsberger et al., 2023; Noël et al., 2023). The misfit could be caused by errors in background altimeter models, however we note we obtain nearly identical results using the alternative dataset of Schröder et al. (2019) and misfit also exists in SMB-corrected GRACE fields (King et al., 2023). A further possible source of the unexplained height signal is ice flow dynamics responding to large-scale climate variability.

The dynamic effect of ice flow and its influence on ice sheet mass and surface elevation at a given point can be estimated from satellite-derived glacier velocities and mass conservation (Supplementary Text S1). The year-on-year changes in ice velocity since 2003 suggest several meters per year of dynamic elevation change. Our analysis shows decadal variations in the lower parts of Pine Island and Thwaites, which could potentially be linked to climate variability and the way the glaciers respond dynamically to variations in ice shelf melt through a combination of advection and strain (Fig. S9).

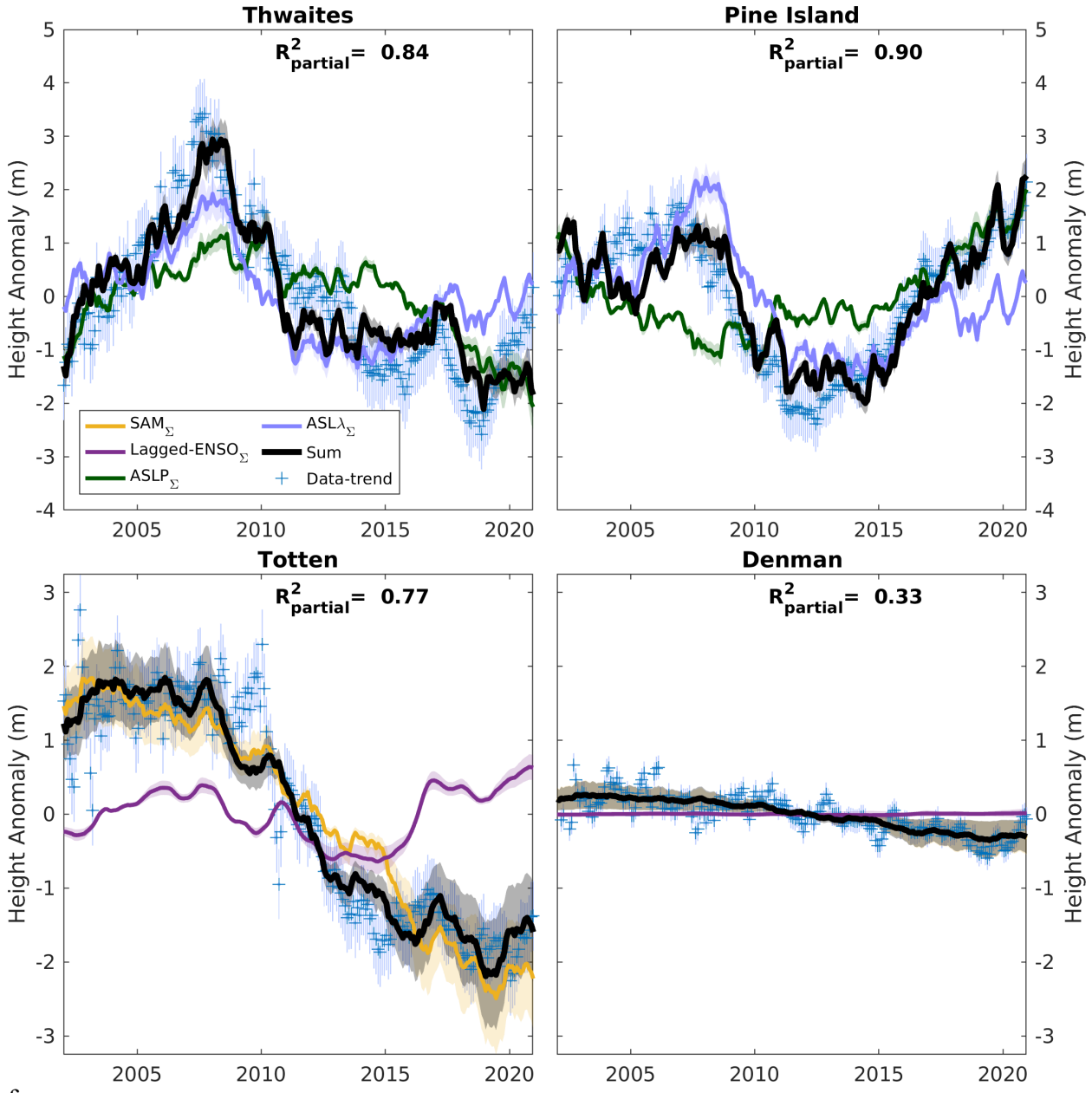

f

Figure 3. Detrended elevation time series at glacier point locations. Time series are shown for sites ~20 km upstream of the grounding line and along the centerline of flow (Fig. S5 yellow crosses; Table S1). Shown are the altimeter time series after 10 km Gaussian smoothing and subtracting the estimated trend and harmonics (blue plusses), and the two components of the model (colored lines) and their sum (black line) for each glacier. For Thwaites and Pine Island glaciers (top row), ASL coefficients are shown, while for Totten and Denman glaciers (bottom row) SAM and ENSO terms are shown. The partial variances explained by the sum of the two coefficients are listed in each panel. Grey shading is the 1-sigma uncertainty of the model. Error bars represent the 2-sigma uncertainties of the data.

3.2.2 Totten and Denman glaciers

The SAM and ENSO coefficients in the region of Totten and Denman glaciers have smaller magnitude and are much more diffuse than in the ASE (Fig. S5d-e). Nonetheless, these terms explain significant amounts of the partial variance (Fig. S5f) in this region. There is almost no non-linear signal to explain near the front of the Denman Glacier (Fig. 3), with the largest SAM or ENSO signal in the Denman region is west of Denman. Nonetheless, SAM contributes about 30% of the partial variance at Denman. If the underlying surface lowering trend of Denman is affected by climate variability it is not obviously associated with SAM and ENSO over this period.

Despite the modest signal near Totten there is still evidence that significant SAM and ENSO signals exist in the fast-flowing region of Totten Glacier (Fig. 3), at least in the 20-30 km above the grounding zone (Fig. S6c, Fig. S7). Unlike the ASE glaciers, there is insufficient ice velocity time series for Totten Glacier to explore the cumulative impacts of time-varying ice dynamics on ice elevation. As noted above, the FDM-corrected results are model-dependent in this region and so the origin(s) of the Totten Glacier non-linear elevation change signal is unclear.

4 Discussion

Our analysis reveals the spatial fingerprints of SAM and ENSO on AIS elevation over 2002-2021, patterns which are confirmed by analysis of GRACE mass change data over the same period. These patterns may not be stationary with time. Indeed, circulation patterns associated with SAM are known to vary over decades (Marshall et al., 2013; Silvestri & Vera, 2009), with effects including variable precipitation in the Antarctic Peninsula (Goodwin et al., 2016). Within this context it is therefore not unexpected that our pattern of SAM variability is different to the SMB-only SAM reconstruction of Medley and Thomas (2019) for the second half of the 20th century for instance. Differences with SMB-only reconstructions would also result if ice-dynamic effects on ice elevation and mass were non-negligible as hinted at by our data.

There are only a few previous studies exploring the relationship between ice dynamics, expressed as changes in ice mass, thickness, or elevation, and modes of climate variability, most notably in the Amundsen Sea Embayment region (Christie et al., 2023). Dutrieux et al. (2014) found reduced PIG ice shelf melt during a strong 2012 La Niña. Consistent with this, Paolo et al. (2018) found PIG ice shelf melting increased during El Niño, reducing ice shelf thickness, but that the ice shelf elevation increased overall due to increased accumulation. The way in which these decadal-scale changes impact upstream ice velocity and integrate with time to thickness and elevation variation requires investigation.

The rate of dynamic thinning or thickening depends on the relative contributions from strain and advection (Supplementary Text S1). At PIG, both factors contributed to sustained thinning of > 2 m per year in 2007-2008 in our analysis (Fig. S9). In 2009, strain switched to thickening while thinning by advection also decreased. Hence, the glacier exhibited net thickening of > 1 m per year during the 2012 La Niña. After 2015, observed velocities suggest the glacier thinned again, mostly due to strain. At Thwaites, strain thinning at rates of 4 m per year or greater outpaces the effect of advection, which is mostly positive (Fig. S9).

The observed height anomalies (Fig. 3) and dynamic elevation change (Fig. S9a,b) do not obviously correlate over the period velocities are available. This may have several explanations. To derive the latter, we assumed surface velocities are constant with depth, which is unlikely to be correct near the bed. Errors in the gridded velocity or ice thickness data also affect these estimates. Fundamentally, upstream ice elevation variability is unlikely to be a simple and immediate linear response to sub ice shelf climate variability (Snow et al., 2017).

The SAM/ASLP-related signal upstream of PIG, Thwaites, and other ASE glaciers is the largest unexplained signal in Antarctica, and it is especially strong at low elevations where atmospheric conditions may drive larger snowfall variations. While there is also a record of ice shelf geometry changes and grounding line retreat there, we suggest the large residual SAM/ASLP signal (Fig. 2) in the ASE is related to SMB and/or firn densification because the ice-dynamic signal which is also present there has a different temporal pattern (compare Fig. 3 with Fig S9c-f).

We note that while the SAM_{Σ} and $ASLP_{\Sigma}$ signals are correlated and our analysis cannot separate their different effects, they have different long-term implications for the ice sheet. As discussed by King et al. (2023), SAM_{Σ} has a trend due to the positive phase of SAM that has emerged since the 1940s. $ASLP_{\Sigma}$ does not have a strong long-term trend, and so the extent to which the changes in coastal West Antarctica are related to the ASL rather than SAM will reduce the inferred contribution of SAM to ice-mass loss over recent decades (King et al., 2023).

Finally, our findings offer a simple way to remove decadal-scale variability from altimetry time series in the presence of imperfect firn densification models. This reduces correlated noise in the time series and will alter both the derived trends and, perhaps most significantly, the uncertainties of derived trends and other parameters if correlated noise is considered in the regression as it should (Ferguson et al., 2004; King & Watson, 2020; Williams et al., 2014; Wouters et al., 2013).

5 Conclusions

We analyzed gridded Antarctic ice elevation time series (2002-2020) and show that much of the time series variance can be explained through a simple linear model based on the cumulative indices of the Southern Annular Mode and El Niño Southern Oscillation. The spatial pattern of this signal, once spatially smoothed, is in close agreement with the spatial pattern evident in GRACE data suggesting that observed ice elevation variability is robust and climatological. The Amundsen Sea Low is more directly relevant to the Amundsen Sea Embayment and we show that variations in its pressure and longitude linearly relate to ~90% of the variance over Pine Island and Thwaites glaciers.

Subtracting the effects of modeled firn densification removes much, but not all, signal, with inter-model differences evident. Residual climatological signal is particularly large at the fronts of fast-flowing glaciers in the Amundsen Sea Embayment. Surface velocity and ice thickness data indicate that ice dynamics make a discernable contribution to decadal variability in

upstream ice elevation. Further work is required to quantify the magnitude and response-times of upstream ice to changes in climatological variability in ice shelf melt.

Acknowledgments

This work was supported by the ARC Australian Centre for Excellence in Antarctic Science (Project ID SR200100008). We thank the individuals and groups sharing altimetry and GRACE data, firn densification models, and climate indices. We thank the Editor, and two anonymous reviewers for thoughtful reviews.

Open Research

Data presented here are available at (King et al., 2023a; King & Christoffersen, 2024). All underlying data are openly available (Brils et al., 2021; Haran et al., 2014, updated 2019; Howat, 2022; Medley et al., 2022a; Morlighem, 2022; Nilsson et al., 2023; Rignot et al., 2017; Sasgen et al., 2020).

References

Bos, M. S., Fernandes, R. M. S., Williams, S. D. P., & Bastos, L. (2013). Fast error analysis of continuous GNSS observations with missing data. *Journal of Geodesy, 87*(4), 351-360. doi:10.1007/s00190-012-0605-0

Brils, M., Kuipers Munneke, P., Van de Berg, W. J., & Van den Broeke, M. (2021). *IMAU-FDM v1.2G GDM release (v1.2G)*. [Dataset]. Zenodo. doi:10.5281/zenodo.5172513

Christie, F. D. W., Steig, E. J., Gourmelen, N., Tett, S. F. B., & Bingham, R. G. (2023). Inter-decadal climate variability induces differential ice response along Pacific-facing West Antarctica. *Nature Communications, 14*(1), 93. doi:10.1038/s41467-022-35471-3

Clem, K. R., Renwick, J. A., & McGregor, J. (2017). Large-Scale Forcing of the Amundsen Sea Low and Its Influence on Sea Ice and West Antarctic Temperature. *Journal of Climate, 30*(20), 8405-8424. doi:10.1175/Jcli-D-16-0891.1

Dahle, C., & Murböck, M. (2020). *Post-processed GRACE/GRACE-FO Geopotential GSM Coefficients COST-G RL01 (Level-2B Product)*. [Dataset]. GFZ Data Services. doi:10.5880/GFZ.GRAVIS_06_L2B

Diener, T., Sasgen, I., Agosta, C., Fürst, J. J., Braun, M. H., Konrad, H., & Fettweis, X. (2021). Acceleration of Dynamic Ice Loss in Antarctica From Satellite Gravimetry. *Frontiers in Earth Science, 9*. Original Research. doi:10.3389/feart.2021.741789

Dutrieux, P., De Rydt, J., Jenkins, A., Holland, P. R., Ha, H. K., Lee, S. H., et al. (2014). Strong Sensitivity of Pine Island Ice-Shelf Melting to Climatic Variability. *Science, 343*(6167), 174-178. doi:doi:10.1126/science.1244341

Ferguson, A. C., Davis, C. H., & Cavanaugh, J. E. (2004). An autoregressive model for analysis of ice sheet elevation change time series. *Ieee Transactions on Geoscience and Remote Sensing, 42*(11), 2426-2436. Article. doi:10.1109/tgrs.2004.836788

Goodwin, B. P., Mosley-Thompson, E., Wilson, A. B., Porter, S. E., & Sierra-Hernandez, M. R. (2016). Accumulation Variability in the Antarctic Peninsula: The Role of Large-Scale

Atmospheric Oscillations and Their Interactions. *Journal of Climate, 29*(7), 2579-2596. doi:10.1175/JCLI-D-15-0354.1

Hansen, N., Langen, P. L., Boberg, F., Forsberg, R., Simonsen, S. B., Thejll, P., et al. (2021). Downscaled surface mass balance in Antarctica: impacts of subsurface processes and large-scale atmospheric circulation. *The Cryosphere, 15*(9), 4315-4333. doi:10.5194/tc-15-4315-2021

Haran, T., Bohlander, J., Scambos, T., & Fahnestock, M. (2014, updated 2019). *MODIS mosaic of Antarctica 2008-2009 (MOA2009) Image Map, Version 1*. [Dataset]. National Snow and Ice Data Center. doi:10.7265/N5KP8037

Horwath, M., Legresy, B., Remy, F., Blarel, F., & Lemoine, J. M. (2012). Consistent patterns of Antarctic ice sheet interannual variations from ENVISAT radar altimetry and GRACE satellite gravimetry. *Geophysical Journal International, 189*(2), 863-876. doi:10.1111/j.1365-246X.2012.05401.x

Hosking, J. S., Orr, A., Bracegirdle, T. J., & Turner, J. (2016). Future circulation changes off West Antarctica: Sensitivity of the Amundsen Sea Low to projected anthropogenic forcing. *Geophysical Research Letters, 43*(1), 367-376. doi:10.1002/2015GL067143

Howat, I. M. (2022). *The Reference Elevation Model of Antarctica – Mosaics, Version 2*. [Dataset]. Harvard Dataverse. doi:10.7910/DVN/EBW8UC

Kaitheri, A., Mémin, A., & Rémy, F. (2021). Inter-Annual Variability in the Antarctic Ice Sheets Using Geodetic Observations and a Climate Model. *Remote Sensing, 13*(11), 2199.

Kappelsberger, M. T., Horwath, M., Buchta, E., Willen, M. O., Schröder, L., Veldhuijsen, S. B. M., et al. (2023). How well can satellite altimetry and firn models resolve Antarctic firn thickness variations? *The Cryosphere Discuss., 2023*, 1-47. doi:10.5194/tc-2023-140

Kim, B.-H., Seo, K.-W., Eom, J., Chen, J., & Wilson, C. R. (2020). Antarctic ice mass variations from 1979 to 2017 driven by anomalous precipitation accumulation. *Scientific Reports, 10*(1), 20366. doi:10.1038/s41598-020-77403-5

King, M., Lyu, K., & Zhang, X. (2023a). *GRACE time series of Antarctic Ice Sheet mass change 2002-2021, and related climate datasets* [Dataset]. Institute for Marine and Antarctic Studies (IMAS), University of Tasmania (UTAS). doi:10.25959/8MW6-ZN03

King, M. A., & Christoffersen, P. (2024). *Gridded SAM and ENSO coefficients derived from satellite altimeter data over the Antarctic Ice Sheet, 2002-2020*. [Dataset]. Institute for Marine and Antarctic Studies (IMAS), University of Tasmania (UTAS). doi:10.25959/MKAIS-D424

King, M. A., Lyu, K., & Zhang, X. (2023b). Climate variability a key driver of recent Antarctic ice-mass change. *Nature Geoscience, 16*(12), 1128-1135. doi:10.1038/s41561-023-01317-w

King, M. A., & Watson, C. S. (2020). Antarctic Surface Mass Balance: Natural Variability, Noise, and Detecting New Trends. *Geophysical Research Letters, 47*(12), e2020GL087493. doi:10.1029/2020GL087493

Marshall, G. J. (2003). Trends in the Southern Annular Mode from Observations and Reanalyses. *Journal of Climate, 16*(24), 4134-4143. doi:10.1175/1520-0442(2003)016<4134:Titsam>2.0.Co;2

Marshall, G. J., Orr, A., & Turner, J. (2013). A Predominant Reversal in the Relationship between the SAM and East Antarctic Temperatures during the Twenty-First Century. *Journal of Climate, 26*(14), 5196-5204. doi:10.1175/Jcli-D-12-00671.1

Medley, B., Neumann, T., Zwally, H. J., Smith, B. E., & Stevens, C. M. (2022a). *NASA GSFC Firn Densification Model version 1.2.1 (GSFC-FDMv1.2.1) for the Greenland and Antarctic Ice Sheets: 1980-2021 (1.2.1)*. [Dataset]. Zenodo. doi:10.5281/zenodo.7054574

Medley, B., Neumann, T. A., Zwally, H. J., Smith, B. E., & Stevens, C. M. (2022b). Simulations of firn processes over the Greenland and Antarctic ice sheets: 1980–2021. *The Cryosphere, 16*(10), 3971-4011. doi:10.5194/tc-16-3971-2022

Medley, B., & Thomas, E. R. (2019). Increased snowfall over the Antarctic Ice Sheet mitigated twentieth-century sea-level rise. *Nature Climate Change, 9*(1), 34-39. doi:10.1038/s41558-018-0356-x

Mémin, A., Flament, T., Alizier, B., Watson, C., & Rémy, F. (2015). Interannual variation of the Antarctic Ice Sheet from a combined analysis of satellite gravimetry and altimetry data. *Earth and Planetary Science Letters, 422*(0), 150-156. doi:10.1016/j.epsl.2015.03.045

Mémin, A., Flament, T., Rémy, F., & Llubes, M. (2014). Snow- and ice-height change in Antarctica from satellite gravimetry and altimetry data. *Earth and Planetary Science Letters, 404*(0), 344-353. doi:10.1016/j.epsl.2014.08.008

Morlighem, M. (2022). *MEaSUREs BedMachine Antarctica, Version 3*. [Dataset]. doi:10.5067/FPSU0V1MWUB6

Mottram, R., Hansen, N., Kittel, C., van Wessem, J. M., Agosta, C., Amory, C., et al. (2021). What is the surface mass balance of Antarctica? An intercomparison of regional climate model estimates. *The Cryosphere, 15*(8), 3751-3784. doi:10.5194/tc-15-3751-2021

Nilsson, J., Gardner, A., & Paolo, a. F. S. (2023). *MEaSUREs ITS_LIVE Antarctic Grounded Ice Sheet Elevation Change, Version 1*. [Dataset]. NASA National Snow and Ice Data Center Distributed Active Archive Center. Retrieved from: https://nsidc.org/data/NSIDC-0782/versions/1 doi:10.5067/L3LSVDZS15ZV

Nilsson, J., Gardner, A. S., & Paolo, F. S. (2022). Elevation change of the Antarctic Ice Sheet: 1985 to 2020. *Earth Syst. Sci. Data, 14*(8), 3573-3598. doi:10.5194/essd-14-3573-2022

Noël, B., van Wessem, J. M., Wouters, B., Trusel, L., Lhermitte, S., & van den Broeke, M. R. (2023). Higher Antarctic ice sheet accumulation and surface melt rates revealed at 2 km resolution. *Nature Communications, 14*(1), 7949. doi:10.1038/s41467-023-43584-6

Otosaka, I. N., Shepherd, A., Ivins, E. R., Schlegel, N. J., Amory, C., van den Broeke, M. R., et al. (2023). Mass balance of the Greenland and Antarctic ice sheets from 1992 to 2020. *Earth Syst. Sci. Data, 15*(4), 1597-1616. doi:10.5194/essd-15-1597-2023

Palóczy, A., Gille, S. T., & McClean, J. L. (2018). Oceanic Heat Delivery to the Antarctic Continental Shelf: Large-Scale, Low-Frequency Variability. *Journal of Geophysical Research: Oceans, 123*(11), 7678-7701. doi:10.1029/2018JC014345

Paolo, F. S., Padman, L., Fricker, H. A., Adusumilli, S., Howard, S., & Siegfried, M. R. (2018). Response of Pacific-sector Antarctic ice shelves to the El Niño/Southern Oscillation. *Nature Geoscience, 11*(2), 121-126. doi:10.1038/s41561-017-0033-0

Rayner, N. A. (2003). Global analyses of sea surface temperature, sea ice, and night marine air temperature since the late nineteenth century. *Journal of Geophysical Research, 108*(D14). doi:10.1029/2002jd002670

Rignot, E., Mouginot, J., & Scheuchl, B. (2017). *MEaSUREs InSAR-Based Antarctica Ice Velocity Map, Version 2*. [Dataset]. NASA National Snow and Ice Data Center Distributed Active Archive Center. doi:10.5067/D7GK8F5J8M8R

Sasgen, I., Groh, A., & Horwath, M. (2020). *COST-G GravIS RL01 Ice-Mass Change Products*. [Dataset]. GFZ Data Services. doi:10.5880/COST-G.GRAVIS_01_L3_ICE

Schröder, L., Horwath, M., Dietrich, R., Helm, V., van den Broeke, M. R., & Ligtenberg, S. R. M. (2019). Four decades of Antarctic surface elevation changes from multi-mission satellite altimetry. *The Cryosphere, 13*(2), 427-449. doi:10.5194/tc-13-427-2019

Shepherd, A., Ivins, E. R., A, G., Barletta, V. R., Bentley, M. J., Bettadpur, S., et al. (2012). A Reconciled Estimate of Ice-Sheet Mass Balance. *Science, 338*(6111), 1183-1189. doi:10.1126/science.1228102

Silvestri, G., & Vera, C. (2009). Nonstationary Impacts of the Southern Annular Mode on Southern Hemisphere Climate. *Journal of Climate, 22*(22), 6142-6148. doi:10.1175/2009JCLI3036.1

Smith, B., Fricker, H. A., Gardner, A. S., Medley, B., Nilsson, J., Paolo, F. S., et al. (2020). Pervasive ice sheet mass loss reflects competing ocean and atmosphere processes. *Science, 368*(6496), 1239-1242. doi:doi:10.1126/science.aaz5845

Snow, K., Goldberg, D. N., Holland, P. R., Jordan, J. R., Arthern, R. J., & Jenkins, A. (2017). The Response of Ice Sheets to Climate Variability. *Geophysical Research Letters, 44*(23), 11878-11885. doi:10.1002/2017gl075745

Spence, P., Holmes, R. M., Hogg, A. M., Griffies, S. M., Stewart, K. D., & England, M. H. (2017). Localized rapid warming of West Antarctic subsurface waters by remote winds. *Nature Climate Change, 7*(8), 595-603. doi:10.1038/nclimate3335

Thomas, E. R., van Wessem, J. M., Roberts, J., Isaksson, E., Schlosser, E., Fudge, T. J., et al. (2017). Regional Antarctic snow accumulation over the past 1000 years. *Clim. Past, 13*(11), 1491-1513. doi:10.5194/cp-13-1491-2017

Turner, J., Phillips, T., Hosking, J. S., Marshall, G. J., & Orr, A. (2013). The Amundsen Sea low. *International Journal of Climatology, 33*(7), 1818-1829. doi:10.1002/joc.3558

van den Broeke, M. R., & van Lipzig, N. P. M. (2017). Changes in Antarctic temperature, wind and precipitation in response to the Antarctic Oscillation. *Annals of Glaciology, 39*, 119-126. doi:10.3189/172756404781814654

Veldhuijsen, S. B. M., van de Berg, W. J., Brils, M., Kuipers Munneke, P., & van den Broeke, M. R. (2023). Characteristics of the 1979–2020 Antarctic firn layer simulated with IMAU-FDM v1.2A. *The Cryosphere, 17*(4), 1675-1696. doi:10.5194/tc-17-1675-2023

Verfaillie, D., Pelletier, C., Goosse, H., Jourdain, N. C., Bull, C. Y. S., Dalaiden, Q., et al. (2022). The circum-Antarctic ice-shelves respond to a more positive Southern Annular Mode with regionally varied melting. *Communications Earth & Environment, 3*(1), 139. doi:10.1038/s43247-022-00458-x

Verjans, V., Leeson, A. A., McMillan, M., Stevens, C. M., van Wessem, J. M., van de Berg, W. J., et al. (2021). Uncertainty in East Antarctic Firn Thickness Constrained Using a Model Ensemble Approach. *Geophysical Research Letters, 48*(7), e2020GL092060. doi:https://doi.org/10.1029/2020GL092060

Wahr, J., Molenaar, M., & Bryan, F. (1998). Time variability of the Earth's gravity field: Hydrological and oceanic effects and their possible detection using GRACE. *Journal of Geophysical Research: Solid Earth, 103*(B12), 30205-30229. doi:10.1029/98JB02844

Wang, B. (1992). The Vertical Structure and Development of the Enso Anomaly Mode during 1979-1989. *Journal of the Atmospheric Sciences, 49*(8), 698-712. doi:10.1175/1520-0469(1992)049<0698:Tvsado>2.0.Co;2

Williams, S. D. P., Moore, P., King, M. A., & Whitehouse, P. L. (2014). Revisiting GRACE Antarctic ice mass trends and accelerations considering autocorrelation. *Earth and Planetary Science Letters, 385*, 12-21. doi:10.1016/j.epsl.2013.10.016

552 Wingham, D. J., Wallis, D. W., & Shepherd, A. (2009). Spatial and temporal evolution of Pine
553 Island Glacier thinning, 1995-2006. *Geophysical Research Letters, 36*, 5. Article.
554 doi:L1750, 10.1029/2009gl039126
555 Wouters, B., Bamber, J. L., van den Broeke, M. R., Lenaerts, J. T. M., & Sasgen, I. (2013).
556 Limits in detecting acceleration of ice sheet mass loss due to climate variability. *Nature*
557 *Geoscience, 6*(8), 613-616. doi:10.1038/ngeo1874
558 Wu, Z. (2023). Empirical Orthogonal Function Toolbox GitHub
559 (https://github.com/zelunwu/eof/releases/tag/v1.2), GitHub. Retrieved May 23, 2023.
560
561
562